Mineralogical Magazine (2019), **83**, 507–514
doi:10.1180/mgm.2019.20

CAMBRIDGE UNIVERSITY PRESS

Article

Twinning and incommensurate modulation in baumoite, $Ba_{0.5}[(UO_2)_3O_8Mo_2(OH)_3](H_2O)_{\sim 3}$, the first natural Ba uranyl molybdate

Peter Elliott[1,2*], Jakub Plášil[3], Václav Petříček[4], Jiří Čejka[5] and Luca Bindi[6,7]

[1]Department of Earth Sciences, School of Physical Sciences, The University of Adelaide, Adelaide, South Australia 5005, Australia; [2]South Australian Museum, North Terrace, Adelaide, South Australia 5000, Australia; [3]Institute of Physics ASCR, v.v.i., Na Slovance 1999/2, 18221 Prague 8, Czech Republic; [4]Institute of Physics, Academy of Sciences of the Czech Republic, v.v.i., Na Slovance 2, 180 40 Praha 8, Czech Republic; [5]Department of Mineralogy and Petrology, National Museum, Cirkusová 1740, 193 00 Praha 9, Czech Republic; [6]Dipartimento di Scienze della Terra, Università di Firenze, Via La Pira 4, I-50121 Firenze, Italy; and [7]CNR–Istituto di Geoscienze e Georisorse, sezione di Firenze, Via La Pira 4, I-50121 Firenze, Italy

ABSTRACT

Baumoite, $Ba_{0.5}[(UO_2)_3O_8Mo_2(OH)_3](H_2O)_{\sim 3}$, is a new mineral found near Radium Hill, South Australia, where it occurs in a granite matrix associated with baryte, metatorbernite, phurcalite and kaolinite. Baumoite forms thin crusts of yellow to orange–yellow tabular to prismatic crystals. The mineral is translucent with a vitreous lustre and pale yellow streak. Crystals are brittle, the fracture is uneven and show one excellent cleavage. The Mohs hardness is ~2½. The calculated density is 4.61 g/cm^3. Optically, baumoite crystals are biaxial (–), with $\alpha = 1.716(4)$, $\beta = 1.761(4)$, $\gamma = 1.767(4)$ (white light); and $2V_{calc} = 42.2°$. Electron microprobe analyses gave the empirical formula $Ba_{0.87}Ca_{0.03}Al_{0.04}U_{2.97}Mo_{2.02}P_{0.03}O_{22}H_{11.99}$, based on 22 O atoms per formula unit. The eight strongest lines in the powder X-ray diffraction pattern are [d_{obs} Å (I) (hkl)]: 9.175(39)(12$\bar{1}$), 7.450(100)(020), 3.554(20)(221), 3.365(31)(004, 202), 3.255(31)(123, 30$\bar{2}$), 3.209(28)(12$\bar{4}$), 3.067(33)(30$\bar{3}$, 222, 32$\bar{2}$) and 2.977(20)(142). Single-crystal X-ray studies ($R_1 = 5.85\%$ for 1892 main reflections) indicate that baumoite is monoclinic, superspace group $X2/m(a0g)0s$ with $X = (0,½,0,½)$, with unit-cell parameters: $a = 9.8337(3)$, $b = 15.0436(5)$, $c = 14.2055(6)$ Å, $\beta = 108.978(3)°$, $V = 1987.25(13)$ Å^3 and $Z = 4$. The crystal structure is twinned and incommensurately modulated and is based upon sheets of U^{6+} and Mo^{6+} polyhedra of unique topology. Four independent cationic sites partially occupied by Ba atoms are located between the sheets, together with H_2O molecules.

Keywords: baumoite, new mineral species, barium uranyl molybdate, incommensurately modulated structure, twinning, Radium Hill

(Received 6 December 2018; accepted 6 March 2019; Accepted Manuscript online: 12 April 2019; Associate Editor: Ian T. Graham)

Introduction

The Olary Province of South Australia hosts a diversity of small uranium deposits (Dickinson *et al.*, 1954; Campana and King, 1958). These include Radium Hill, Crocker's Well, Mt Victoria and several smaller prospects. Most of the deposits are low grade and the only significant production has been from Radium Hill which was Australia's first uranium mine, discovered in 1906 and operated until 1961. The deposits are intrusive-type deposits, associated with Mesoproterozoic intrusives, mainly granite, alaskite, pegmatite and migmatite. The primary minerals are davidite-(La) and brannerite and only a small number of secondary uranium minerals have been recorded. Secondary uranium minerals have also been reported from numerous pegmatites and granites in the region and it is one of these that has produced the specimens containing baumoite. Baumoite is one of nine uranyl molybdate minerals and the first natural Ba, uranyl molybdate. Its structure is twinned and incommensurately modulated, one of several U^{6+} modulated structures that have been discovered recently along with swamboite-(Nd) and shinkolobweite (Olds *et al.*, 2017; Plášil *et al.*, 2017; Plášil, 2018). Despite the weak intensities of the satellite reflections (only those of the 1st order were detected) on the CCD frames, the refinement in superspace converged to the reasonable values and it provided a reasonable structure model. Baumoite is named for its chemical composition. The mineral and its name have been approved by the Commission on New Minerals, Nomenclature and Classification of the International Mineralogical Association (IMA2017-054, Elliott *et al.*, 2017). The holotype specimen of baumoite is deposited in the mineral collection of the South Australian Museum, Adelaide, South Australia (registration number G34697).

Occurrence

The Olary Domain is contained within the Curnarnona Province that extends across northeastern South Australia and western New South Wales. The geology comprises a late Palaeoproterozoic metasedimentary and metavolcanic succession (Willyama Supergroup)

*Author for correspondence: Peter Elliott, Email: peter.elliott@adelaide.edu.au
Cite this article: Elliott P., Plášil J., Petříček V., Čejka J. and Bindi L. (2019) Twinning and incommensurate modulation in baumoite, $Ba_{0.5}[(UO_2)_3O_8Mo_2(OH)_3](H_2O)_{\sim 3}$, the first natural Ba uranyl molybdate. *Mineralogical Magazine* **83**, 507–514. https://doi.org/10.1180/mgm.2019.20

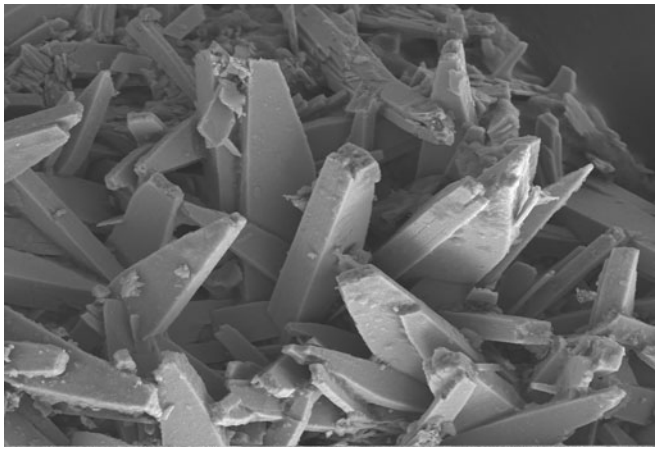

Fig. 1. Scanning electron microscopy photomicrograph showing crystals of baumoite. The field of view is 100 mm across.

with some meta-intrusives and early Mesoproterozoic volcanics and granitoid intrusives (Stevens, *et al.*, 1990; Flint and Parker, 1993). The lithological and geophysical character of the Willyama Supergroup in the Olary Domain differs from the remainder of the Province with a higher proportion of shallow water sediments, lesser volcanics, widespread metasomatism, particularly albitisation, and an abundance of syntectonic to late-tectonic granitoids (Callen, 1990; Forbes, 1991; Flint and Parker, 1993). Rocks in the Radium Hill area are metasedimentary quartz–feldspathic gneiss, composite gneiss, quartz–feldspar–biotite schist and amphibolite of the Willyama Supergroup. Granitoid intrusives crop-out to the northwest of Radium Hill. Baumoite was found as thin crusts of minute crystals in thin seams on specimens collected in the late 1980s from a weathered granite outcrop, 4 km NW of the Radium Hill mine. Associated minerals are baryte, metatorbernite, phurcalite and kaolinite. The granite comprises pink orthoclase, quartz and muscovite. Baumoite has resulted from the alteration of baryte and primary U and Mo minerals by oxidising groundwaters. No primary U and Mo minerals have been observed in specimens containing baumoite, however, rocks in the surrounding area contain uraninite, davidite-(La) and molybdenite.

Appearance, physical and optical properties

Baumoite occurs as yellow to orange-yellow tabular to prismatic crystals up to 0.11 mm in size (Fig. 1). Crystals are translucent with a vitreous lustre, pale yellow streak, and show bright yellow green fluorescence under shortwave ultraviolet illumination. The Mohs hardness is ~2½. The density could not be measured as it exceeds that of available heavy liquids; the calculated density is 4.61 g/cm^3 from the empirical formula and 4.68 g/cm^3 from the ideal formula. Baumoite is brittle, the fracture is uneven and shows one excellent cleavage. Baumoite is optically biaxial (–), $\alpha = 1.716(4)$, $\beta = 1.761(4)$ and $\gamma = 1.767(4)$ measured in white light. Calculated 2V is 42.2°. The Gladstone–Dale compatibility index is 0.009, classed as excellent (Mandarino, 1981).

Infrared spectroscopy

The infrared spectrum (Fig. 2) of powdered baumoite in the range 4000 to 650 cm^{-1} was obtained using a Nicolet 5700 FTIR spectrometer equipped with a Nicolet Continuum IR microscope and a diamond-anvil cell. The spectrum was interpreted with regard to the theoretical and experimental papers published by Hardcastle and Wachs (1990), Fomichev *et al.* (1992), Čejka (1999), Fedoseev *et al.* (2001), Sidorenko *et al.* (2005), Frost *et al.* (2008), Mączka *et al.* (2009), Nakamoto (2009), Zhang and Guo (2012) and Barik *et al.* (2014). Moreover, we used data taken from Katscher *et al.* (1990), who reviewed infrared and/or Raman spectra of $(MoO_x)^{n-}$ units in synthetic and mineral phases. Two bands at 3699 (vw) and 3489 (sb) and a shoulder at 3263 cm^{-1} are assigned to the ν OH stretching vibrations of hydrogen bonded to water molecules and hydrogen bonded

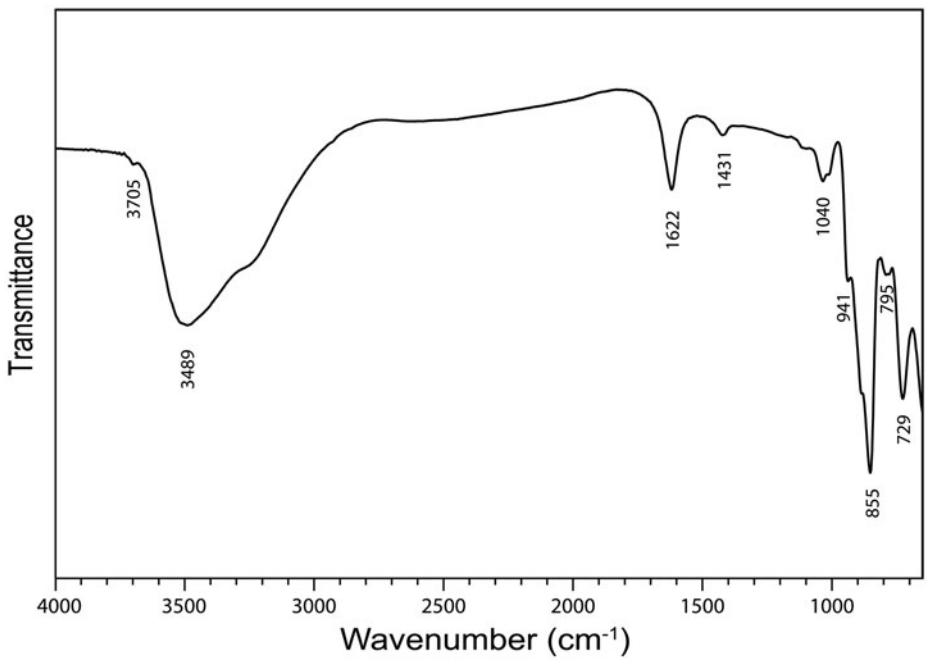

Fig. 2. Fourier-transform infrared spectrum of powdered baumoite.

Table 1. Compositional data for baumoite.

Constituent	Weight %	Range	Standard deviation
BaO	9.88	8.80–11.38	0.73
CaO	0.12	0.08–0.19	0.03
Al_2O_3	0.14	0.07–0.39	0.07
UO_3	62.80	60.50–65.61	1.29
MoO_3	21.56	20.36–22.64	0.67
P_2O_5	0.15	0.06–0.81	0.18
H_2O (calc)*	7.99		
Total	102.64		

*calculated to obtain charge balance.

hydroxyls. According to Libowitzky (1999), approximate O–H···O hydrogen bond lengths vary from >3.2 to 2.73 Å. A medium strong band at 1616 cm^{-1} is attributed to the ν_2 (δ) H_2O bending vibration and weak bands at 1417 (shoulder), 1171 (vvw), 1100 (sh), 1030 (w-m), 1013 (w-m) may be connected with U–OH bending vibrations. A shoulder at 934 cm^{-1} and a very strong band at 851 cm^{-1} together with a shoulder at 880 cm^{-1} are attributed to the ν (Mo–O) stretching vibrations (Katscher *et al.*, 1990). However, an overlap (a coincidence) of this vibration with the ν_3 $(UO_2)^{2+}$ antisymmetric stretching vibration is assumed. A shoulder at 787 cm^{-1} is connected with the ν_1 $(UO_2)^{2+}$ antisymmetric stretching vibration. According to Bartlett and Cooney (1989), approximate U–O bond lengths in uranyl, inferred from the wavenumbers of the $(UO_2)^{2+}$ stretching vibrations, are 1.82 Å (based on ν_3) and 1.82 Å (based on ν_1). Observed lengths are somewhat higher than the U–O lengths in uranyl ~1.8 Å, proposed by Lussier *et al.* (2016). A strong band at 723 cm^{-1} is attributable to the ν (Mo_2O_2) stretching vibration of the Mo = O_2 = Mo unit bridging two Mo-octahedra and thus forming (Mo_2O_2) units (Katscher *et al.*, 1990).

Table 2. Powder X-ray diffraction data for baumoite.

I_{obs}	I_{calc}*	d_{obs}	d_{calc}	*h k l*
39	**31**	**9.175**	**9.269**	**1 0 $\bar{1}$**
100	**100**	**7.450**	**7.548**	**0 2 0**
10	4	6.707	6.733	1 0 1
6	1	5.784	5.853	1 2 $\bar{1}$
	2		4.966	2 0 $\bar{1}$
4	1	4.642	4.634	2 0 $\bar{2}$
4	1	4.084	4.041	1 2 2
3	1	3.938	3.949	2 2 $\bar{2}$
9	11	3.764	3.774	0 4 0
17	1	3.705	3.635	0 4 $\bar{1}$
20	19	3.554	3.559	2 2 1
4	1	3.456	3.501	1 4 0
31	**12, 16**	**3.365**	**3.378, 3.367**	**0 0 4, 2 0 2**
31	**10, 6**	**3.255**	**3.264, 3.279**	**1 2 3, 3 0 $\bar{2}$**
28	**36**	**3.209**	**3.232**	**1 2 $\bar{4}$**
33	**11, 24, 11**	**3.067**	**3.090, 3.075, 3.008**	**3 0 $\bar{3}$, 2 2 2, 3 2 $\bar{2}$**
20	17	2.977	2.963	1 4 2
1	1	2.826	2.817	2 0 3
	1	2.694	2.698	1 2 4
2	1	2.587	2.601	2 2 $\bar{5}$
3	2	2.497	2.512	2 4 2
1	1	2.439	2.475	3 4 $\bar{2}$
1	1	2.283	2.283	1 2 5
1	1	2.243	2.249	2 2 $\bar{6}$
3	1	2.040	2.042	1 0 6
2	1	1.993	1.975	4 4 $\bar{4}$
3	1	1.966	1.967	2 2 $\bar{7}$
2	1	1.862	1.862	2 6 $\bar{5}$
1	1	1.806	1.810	2 0 6
1	1	1.789	1.792	4 2 3
1	1	1.728	1.730	5 4 $\bar{1}$

*Calculated intensities were obtained using the program *Rietica* (Hunter, 1998).
The strongest lines are given in bold

Chemical composition

The chemical composition of baumoite (20 points on one crystal aggregate) was determined using a Cameca SXFive electron microprobe operating in the wavelength-dispersive mode with an acceleration voltage of 20 kV, beam current of 20 nA, and 5 μm beam diameter. Data were processed using the φ(ϱz) correction procedure of Pouchou and Pichoir (1985). Analytical data (average of 20 points) are given in Table 1. The standards employed were: baryte (Ba), wollastonite (Ca), almandine (Al), U-metal (U), Mo-metal (Mo), and apatite (P). The empirical formula, calculated on the basis of 22 oxygen atoms and with H_2O calculated to obtain charge balance, is $Ba_{0.87}Ca_{0.03}$ $Al_{0.04}U_{2.97}Mo_{2.02}P_{0.03}O_{22}H_{11.99}$. The simplified formula is BaU_3 $Mo_2O_{16}(H_2O)_6$.

X-ray crystallography

Powder X-ray diffraction

Powder X-ray studies (Table 2) were carried-out using a Rigaku Hiflux Homelab diffractometer, with monochromatised Cu*K*α radiation (λ = 1.541870 Å). Unit-cell parameters refined using the Le Bail profile-fitting method (Le Bail *et al.*, 1988; Hunter, 1998) and starting from the unit-cell parameters determined from the single-crystal study (see below), are a = 9.921(1), b = 15.080(1), c = 14.295(2) Å, β = 109.279(5)° and V = 2018.7(3) $Å^3$.

Single-crystal X-ray diffraction

The single-crystal X-ray study was carried-out using intensity data collected at 293 K on a Rigaku SuperNova diffractometer (Mo*K*α radiation from the microfocus X-ray tube, β = 0.71070 Å) equipped with an Atlas S2 CCD detector using a crystal 0.065 mm × 0.045 mm × 0.01 mm in size. Initial attempts to solve and refine the structure based on the preliminary data from an Oxford Diffraction Xcalibur E diffractometer (Mo*K*α radiation from the conventional X-ray tube, λ = 0.71070 Å) equipped with an EoS CCD were done in the monoclinic space group *C*2/*m*, but this refinement returned only poor *R* values (R_1 ≈ 0.10 with a significantly large GoF ≈ 4), thus representing an average structure. By the careful inspection of the diffraction data it was found that the structure of baumoite is twinned and incommensurately modulated. The satellite reflections can be described by the modulation vector $\mathbf{q} = 0.718\mathbf{a}^* + 0.2803\mathbf{c}^*$. Twin domains are related by the two-fold rotation along [001] axis represented by the twinning matrix [–1 0 –0.451/0 –1 0/0 0 1], which leads to a partial overlap of the reflections. Corrections for background, Lorentz, and polarisation effects were applied to the data during reduction in the *CrysAlis* package (Rigaku, 2018). The final data set was integrated as an *hklm* file (for the commensurate *3 + 1* case) using *CrysAlis* based on the list of reflections generated in *Jana2006* (Petříček *et al.*, 2014). A correction for absorption was done using spherical harmonics by the *Jana2006* program. Refinement of the modulated structure in the superspace group $X2/m(a0g)0s$ with X = (0,½,0,½) was started using the atom coordinates obtained from the average

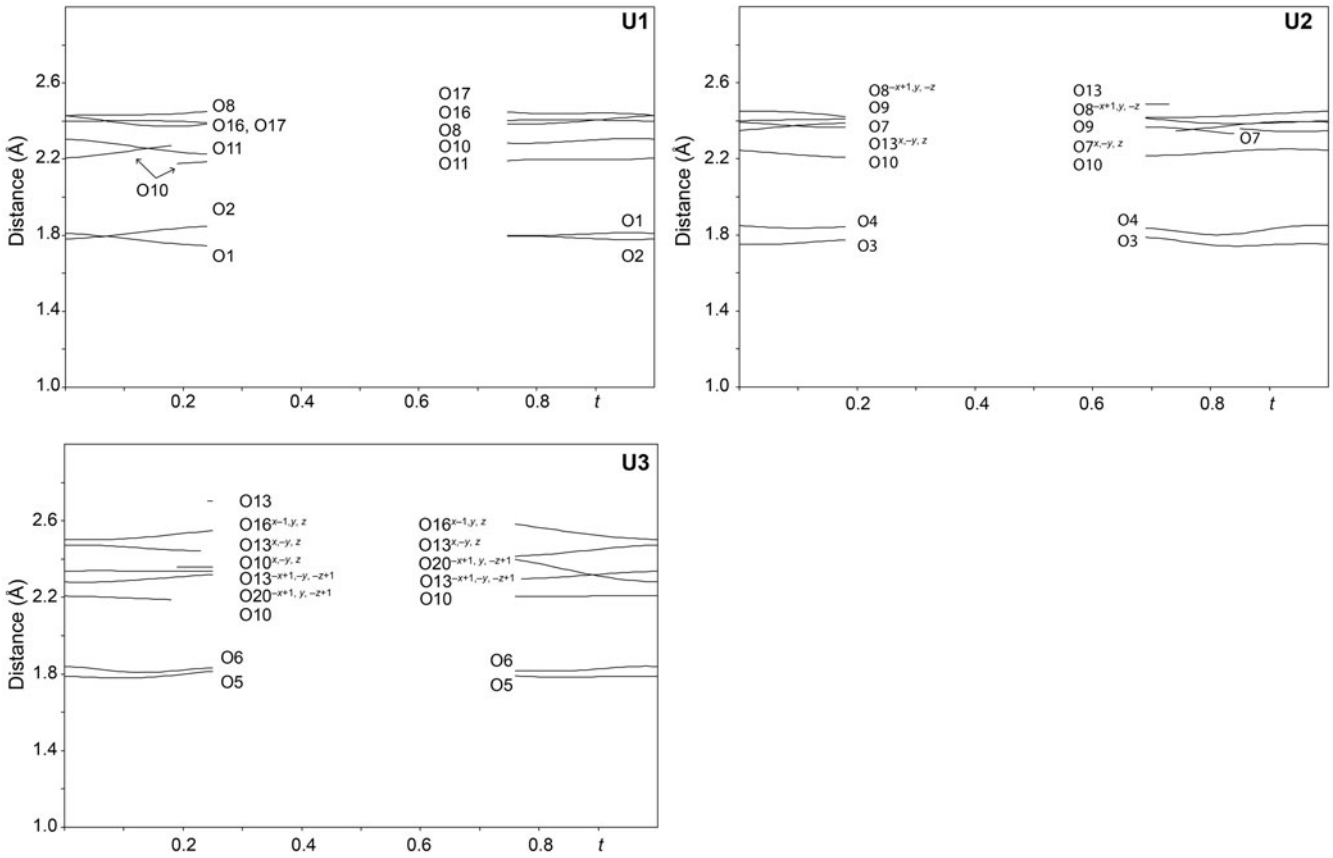

Fig. 3. Bond distances around U1, U2 and U3 sites in the incommensurately modulated structure of baumoite as a function of the internal coordinate *t*.

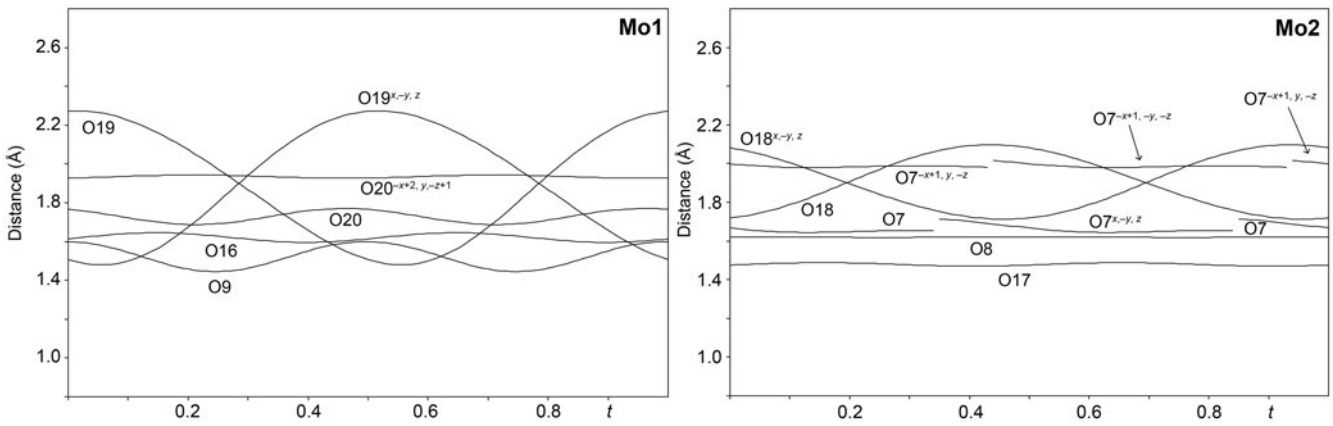

Fig. 4. Bond distances around the Mo1 and Mo2 sites in the incommensurately modulated structure of baumoite as a function of the internal coordinate *t*.

structure solved by *Superflip* (Palatinus and Chapuis, 2007). One modulation wave was set for the refinement. The modulations in the structure of baumoite were described using both continuous (harmonics) and discontinuous (crenel-like; Petříček *et al.*, 2016) modulation functions. There are strong positional modulations of the U, Mo and O atoms that are linked to previously mentioned atoms and a strong occupational modulation of the Ba atoms and also less positional modulation of the Ba atoms and O atoms of the H_2O sites. We have used the recently developed refinement technique in which the refinement is repeated

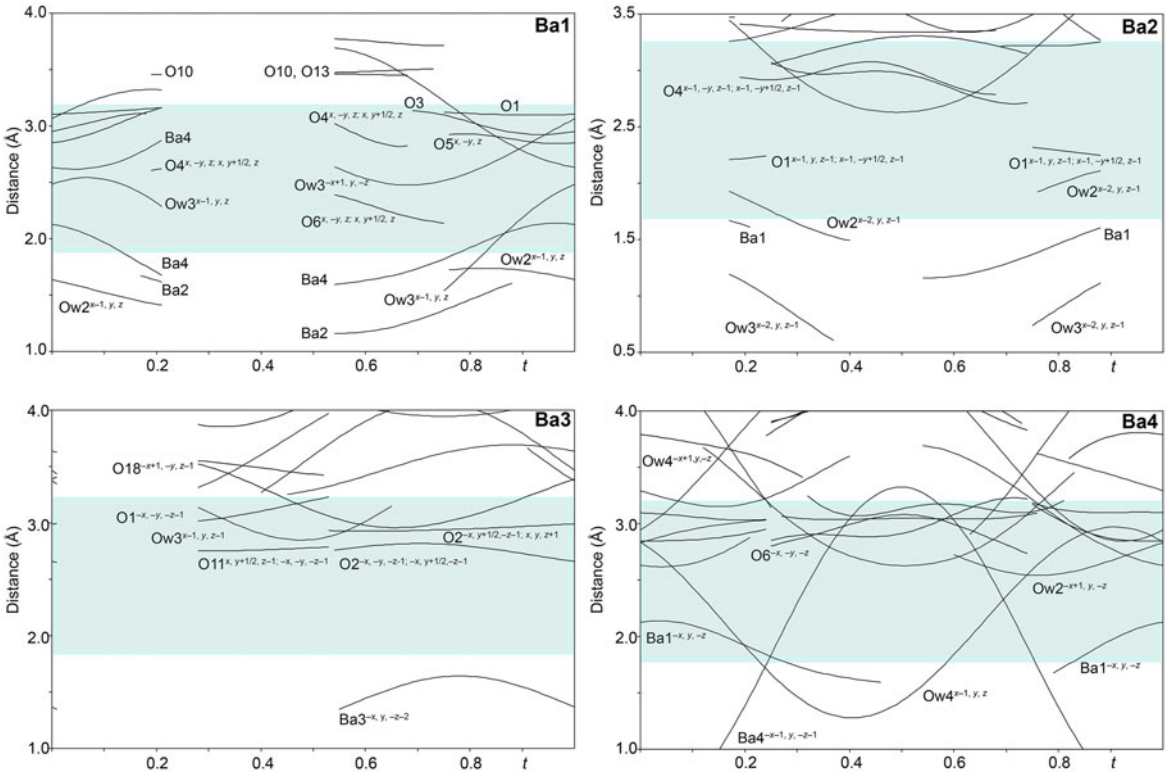

Fig. 5. Bond distances around the Ba sites in the incommensurately modulated structure of baumoite as a function of the internal coordinate *t*. The bluish region highlights the range of the most typical Ba–O distances in the crystalline solids.

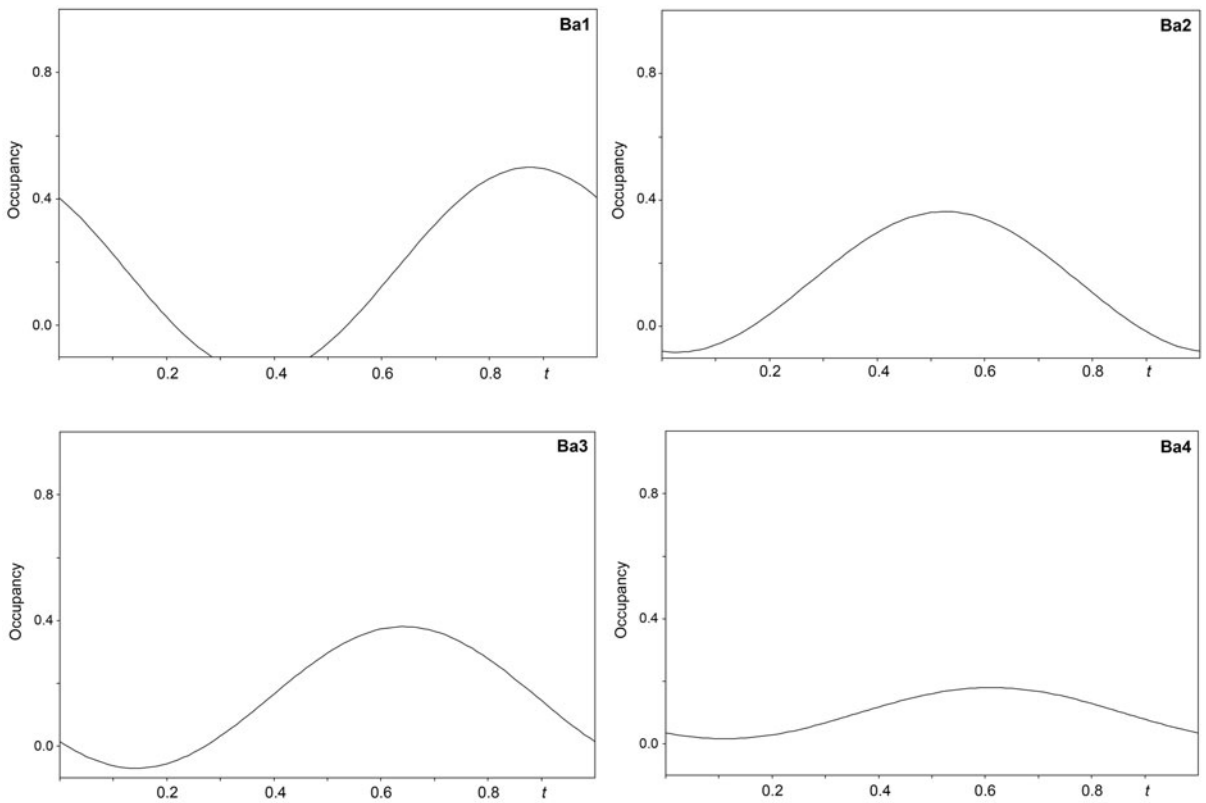

Fig. 6. Refined occupancies of the Ba sites in the incommensurately modulated structure of baumoite as a function of the internal coordinate *t*.

Table 3. Crystallographic and refinement parameters for baumoite.

Crystal data	
Chemical formula	$Ba_{0.56}U_3Mo_2O_{19.72}H_{8.4}$
Temperature (K)	293
Cell setting	Monoclinic
Superspace group	$X2/m(\alpha 0\gamma)0s$
a, *b*, *c* (Å)	9.8337(3), 15.0436(5), 14.2055(6)
β (°)	108.978(3)
V (Å^3)	1987.25(13)
Z	4
Modulation wave vector	**q** = 0.718(4)**a*** + 0.280(2)**c***
Calculated density (g cm^{-3})	4.61
μ (mm^{-1})	26.777
Data collection	
Diffractometer	Rigaku SuperNova with Atlas S2 CCD
Radiation type, wavelength (Å)	Mo*K*α, 0.71073
No. of measured, independent and observed [$I > 2\sigma(I)$] reflections	41859, 6953, 4521
Range of *h*, *k*, *l*, *m*	$-13 \rightarrow h \rightarrow 13$ $-19 \rightarrow k \rightarrow 19$ $-18 \rightarrow l \rightarrow 18$ $-1 \rightarrow m \rightarrow 1$
T_{min}, T_{max}	0.462, 1
No. of main reflections	2442
No. of 1st order satellite reflections	4511
Criterion for observed reflections	$I > 3\sigma(I)$
R_{int}	0.064
Refinement	
Refinement on	*F*
R_{obs}, wR_{obs} (all reflections)	0.0702, 0.0771
R_{obs}, wR_{obs} (main reflections)	0.0585, 0.0645
R_{obs}, wR_{obs} (satellites) 1st order	0.0855, 0.0936
S_{obs}/all	2.71/2.33
No. of parameters	252
$\Delta\rho_{max}$, $\Delta\rho_{min}$ (e^- Å^{-3})	9.51, −5.57
Twin fraction	0.950(4)/0.050(4)
Weights	$1/(\sigma^2(F) + 0.0001F^2)$

several times starting from small randomly chosen modulation amplitudes. Crystallographic details, data collection and refinement parameters for the average and incommensurate structures, respectively, are given in Table 3. Fractional coordinates and atom displacement parameters, Fourier amplitudes of the occupational modulation are given in the accompanying crystallographic information files, which have been deposited with the Principal Editor of *Mineralogical Magazine* and are available as Supplementary material (see below). Selected interatomic distances as functions of *t* are displayed on Figs 3, 4 and 5; refined occupancies of Ba sites are displayed on Fig. 6.

Results and discussion

Description of the structure

The structure of baumoite contains three symmetrically distinct U sites, two Mo sites, four Ba sites and 22 O sites. All U sites in the structure are [7]-fold coordinated in the form of a pentagonal bipyramid, consisting of two strong U–O bonds, i.e. forming uranyl ion $(UO_2)^{2+}$, and five weaker bonds distributed in the equatorial plane of the pentagonal bipyramid (Fig. 3). All U in baumoite is present as hexavalent. The two Mo sites are [6]-coordinated in the form of irregular, distorted octahedra (Fig. 4). The Mo1 and Mo2 polyhedra share their common edge to form $Mo_2\varphi_{10}$ dimers. The baumoite structure is based upon uranyl-molybdate sheets. The fundamental building blocks of the sheets are trimers of edge-sharing U1, U2 and U3 polyhedra,

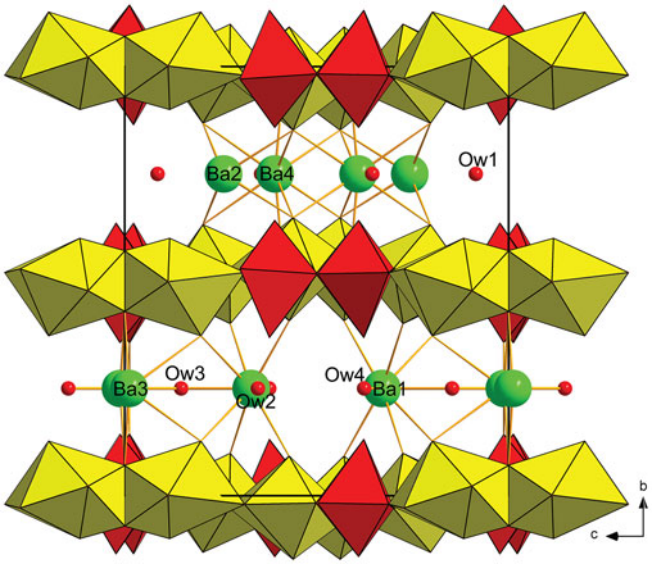

Fig. 7. Approximant structure of baumoite at $t = 0$. Uranyl-molybdate sheets, composed of uranyl pentagonal bipyramids (yellow) and Mo^{6+}-octahedra (red), are alternating interlayer, where Ba atoms (green) and H_2O molecules (Ow1–4) are localised.

which further share a common edge with other symmetrically related U3 polyhedra to form the six-membered clusters (Figs 7, 8*a*). These clusters are connected through the O11 equatorial atom of the U1 bipyramid to form irregular chains propagated along [$\bar{1}$01]. These chains of polyhedra are connected through $Mo_2\varphi_{10}$ dimers in a stair-case-like way (Fig. 8*a*).

Adjacent sheets are separated from each other at an interplanar distance of 7.5 Å (corresponding to half of the **b**-cell parameter). Between the sheets four symmetrically independent Ba atoms and four symmetrically independent H_2O molecules are localised. All the Ba atoms are strongly occupationally and positionally modulated (Figs 5 and 6). The O sites of the corresponding H_2O molecules are both occupationally and positionally modulated; the amplitude of their modulation depends on the presence of the corresponding Ba (to which they are coordinated) or presence of the under-and above-laying U-Mo sheet fragments.

Baumoite topology

Sheets in the structure of baumoite are topologically unique, when considering an approximant, idealised structure (Fig. 7). Another structure with similar high U:Mo ratio is a synthetic phase with composition $Ag_{10}[(UO_2)_8O_8(Mo_5O_{20})]$ (Krivovichev and Burns, 2003); however, in that phase there are infinite complex chains of edge-sharing pentagonal uranyl bipyramids which are linked through Mo_2O_7 dimers, as a part of Mo_5O_{20} interconnecting adjacent sheets (with interplanar spacing ≈ 6.5 Å) (Fig. 8*c*). Another structure containing similar sheets with isolated dimers of Mo-octahedra (within the sheets) is that of synthetic $K_2Na_8(UO_2)_8Mo_4O_{24}[(S,Mo)O_4]$ (Krivovichev, 2014). All the mentioned molybdates are monoclinic.

Incommensurate modulation in baumoite most probably results from long-range positional ordering of Ba, U and Mo atoms. The nature of the baumoite structure resembles the behaviour of composite structures, known for sulfosalts (Petříček *et al.*,

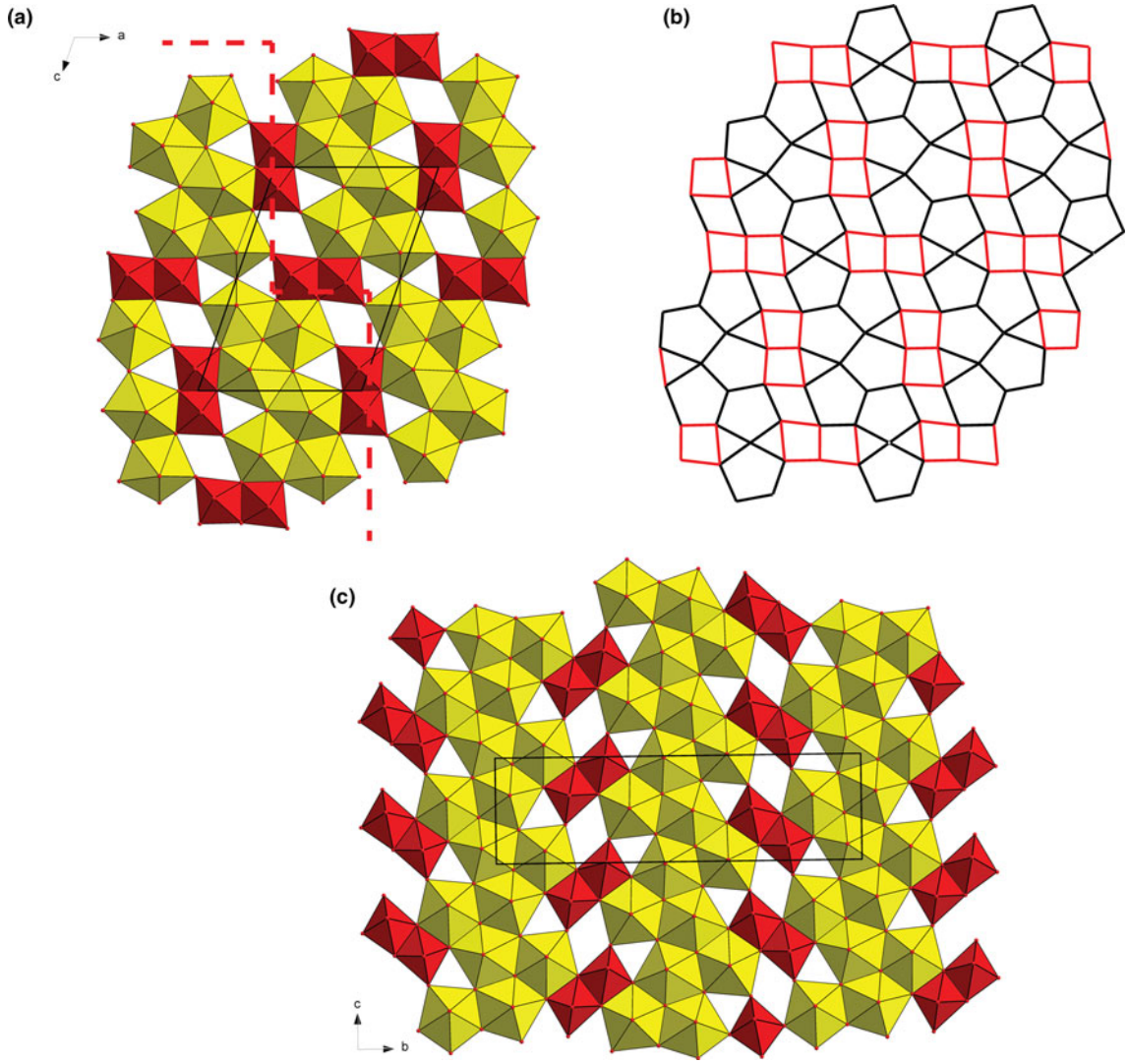

Fig. 8. Structural sheets in uranyl molybdates. (*a*) Uranyl molybdate sheet in baumoite at $t = 0$. UO_7 bipyramids (yellow) share edges and vertices to form irregular infinite ribbons interconnected through dimers of Mo polyhedra (red), running through as stairs-like (represented by a dashed line). (*b*) Corresponding representation of the baumoite uranyl-anion topology. (*c*) Sheet in synthetic $Ag_{10}[(UO_2)_8O_8(Mo_5O_{20})]$ (Krivovichev and Burns, 2003).

1991; Makovicky *et al.*, 2011; Jaszczak *et al.*, 2016). Such structures are based on two, interpenetrating lattice-periodic structures that are mutually incommensurate. Nevertheless, in the case of baumoite, it was not possible to check for such a possibility by the refinement due to limited quality of the data (only satellites of the first order were observed).

The idealised formula of baumoite inferred from the results of the structure refinement and bond-valence considerations is $Ba_{0.5}[(UO_2)_3O_8Mo_2(OH)_3](H_2O)_{\sim 2.72}$ with $Z = 4$. However, from the refinement, it is clear that the picture is much more complex, as some of the O atoms within the equatorial plane of the U polyhedra are in fact protonated (as OH) and some of them can also be H_2O in some regions of the superspace. This corresponds to the regions where Ba positions are not fully occupied, therefore the structure sheets tend to be electroneutral with an approximate composition $[(UO_2)_3O_6Mo_2(OH)_4(H_2O)_{\sim 1.0}]^0$.

Acknowledgements. We are grateful to Vince Peisley and Glynn Francis for supplying us with specimens of baumoite. Ben Wade of Adelaide Microscopy, The University of Adelaide is thanked for assistance with the microprobe analysis. The infrared spectrum was acquired with the assistance of the Forensic Science Centre, Adelaide. JP and VP acknowledge the support through the project No. LO1603 under the Ministry of Education, Youth and Sports National sustainability program I of the Czech Republic. The authors thank Stuart Mills, Peter Leverett and two anonymous reviewers for helpful suggestions which improved the manuscript.

Supplementary material. To view supplementary material for this article, please visit https://doi.org/10.1180/mgm.2019.20.

References

Barik S.K., Chatterjee S. and Choudhary R.P.N. (2014) Molecular and impedance spectrosocpy of $Na_2Mo_2O_7$ ceramics. *Praman – Journal of Physics*, **83**, 571–577.

Bartlett J.R. and Cooney R.P. (1989) On the determination of uranium-oxygen bond lengths in dioxouranium(VI) compounds by Raman spectroscopy. *Journal of Molecular Structure*, **193**, 295–300.

Callen R.A. (1990) *Curnamona, South Australia, sheet SH/54-14*. South Australia Geological Survey 1:250 000 Series Explanatory Notes.

Campana B. and King D. (1958) Regional Geology and Mineral Resources of the Olary Province. *Geological Survey of South Australia, Bulletin*, **34**, 133 p.

Čejka J. (1999) Infrared spectroscopy and thermal analysis of the uranyl minerals. Pp. 521–622 in: *Uranium: Mineralogy, Geochemistry and the Environment* (P.C. Burns and R. Finch, editors). Reviews in Mineralogy, **38**. Mineralogical Society of America, Chantilly, Virginia, USA.

Dickinson S.B., Sprigg R.C., King D., Wade M.L., Webb B.P. and Whittle A.W.G. (1954) Uranium Deposits in South Australia. *Geological Survey of South Australia Bulletin*, **30**, 151 p.

Elliott P., Plášil J., Petříček V., Čejka J. and Bindi L. (2017) Baumoite, IMA 2017-054. CNMNC Newsletter No. 39, October 2017, page 1282; *Mineralogical Magazine*, **81**, 1279–1286.

Fedoseev A.M., Budantseva N.A., Shirokova I.B., Andreev G.B., Yurik T.K. and Krupa J.C. (2001) Synthesis and physicochemical properties of uranyl molybdate complexes of ammonium, potassium, rubidium, and cesium ions. *Russian Journal of Inorganic Chemistry*, **46**, 40–43.

Flint D.J. and Parker A.J. (1993) Willyama Inliers. Pp. 82–93 in: *The Geology of South Australia, vol. I, The Precambrian*. (J.F. Drexel, W.V. Preiss and A.J. Parker, editors). South Australia Geological Survey, Bulletin, **54**.

Fomichev V.V., Poloznikova M.E. and Kondratova O.I. (1992) Structure features, spectroscopic and energy characteristics of alkali metal molybdates and tungstates. *Uspekhi Khimii*, **61**, 1601–1622.

Forbes B.G. (1991) *Olary, South Australia, sheet SI 54-2*. South Australia Geological Survey I: 250 000 Series Explanatory Notes.

Frost R.L., Čejka J. and Dickfos M.J. (2008) Raman and infrared spectroscopic study of the molybdate-containing uranyl mineral calcurmolite. *Journal of Raman Spectroscopy*, **39**, 779–785.

Hardcastle F.D. and Wachs I. (1990) Determination of molybden-oxygen bond distance and bond orders by Raman spectroscopy. *Journal of Raman Spectroscopy*, **21**, 683–691.

Hunter B.A. (1998) Rietica – A Visual Rietveld Program. *Commission on Powder Diffraction Newsletter*, **20**, 21.

Jaszczak J.A., Rumsey M.S., Bindi L., Hackney S.A., Wise M.A., Stanley C.J. and Spratt J. (2016) Merelaniite, $Mo_4Pb_4VSbS_{15}$, a new molybdenum-essential member of the cylindrite group, from the Merelani tanzanite deposit, Lelatema Mountains, Manyara Region, Tanzania. *Minerals*, **6**, 115.

Katscher H., Jehn H. and Kurtz W. (editors) (1990) *Gmelin Handbook of Inorganic Chemistry*, 8th Edition, Mo Supplement Vol. B5, p. 218–220. Springer, Berlin-Heidelberg.

Krivovichev S.V. (2014) $K_2Na_8(UO_2)_8Mo_4O_{24}[(S,Mo)O_4]$, the first uranium molybdosulfate: synthesis, crystal structure, and comparison to related compounds. *Journal of Geosciences*, **59**, 115–121.

Krivovichev S.V. and Burns P.C. (2003) Crystal chemistry of uranyl molybdates. X. The crystal structure of $Ag_{10}[(UO_2)_8O_8(Mo_5O_{20})]$. *The Canadian Mineralogist*, **41**, 1455–1462.

Le Bail A., Duroy H. and Fourquet J.L. (1988) Ab-initio structure determination of $LiSbWO_6$ by X-ray powder diffraction. *Materials Research Bulletin*, **23**, 447–452.

Libowitzky E. (1999) Correlation of O–H stretching frequencies and O–H···O hydrogen bond lengths in minerals. *Monatshefte für Chemie*, **130**, 1047–1059.

Lussier A.J., Lopez R.A.K. and Burns P.S. (2016) A revised and expanded structure hierarchy of natural and synthetic hexavalent uranium compounds. *The Canadian Mineralogist*, **54**, 177–283.

Mączka M., Pietraszko A., Paraguassu W., Souza Filho A.G., Freire P.T.C., Mendes Filho J. and Hanuza J. (2009) Strucural and vibrational properties of $K_3Fe(MoO_4)(Mo_2O_7)$ – a novel layered molybdate. *Journal of Physics: Condensed Matter*, **21**, 1–8.

Makovicky E., Petříček V., Dušek M. and Topa D. (2011) The crystal structure of franckeite, $Pb_{21.7}Sn_{9.3}Fe_{4.0}Sb_{8.1}S_{56.9}$. *American Mineralogist*, **96**, 1686–1702.

Mandarino J.A. (1981) The Gladstone-Dale relationship: Part IV: The compatibility concept and its application. *The Canadian Mineralogist*, **19**, 441–450.

Nakamoto K. (2009) *Infrared and Raman Spectra of Inorganic and Coordination Compounds Part A. Theory and Applications in Inorganic Chemistry*. Wiley and Sons, Hoboken, USA.

Olds T.A., Lussier A.J., Oliver A.G., Petříček V., Plášil J., Kampf A.R., Burns P.C., Dembowski M., Carlson S.M. and Steele I.M. (2017) Shinkolobweite, IMA 2016-095. CNMNC Newsletter No. 36, April 2017, page 404; *Mineralogical Magazine*, **81**, 403–409.

Palatinus L. and Chapuis G. (2007) Superflip – a computer program for the solution of crystal structures by charge flipping in arbitrary dimensions. *Journal of Applied Crystallography*, **40**, 451–456.

Petříček V., Malý K., Coppens P., Bu X., Císařová I and Frost-Jensen A. (1991) The description and analysis of composite crystals. *Acta Crystallographica*, **A47**, 210–216.

Petříček V., Dušek M. and Palatinus L. (2014) Crystallographic computing system JANA2006: general features. *Zeitschrift für Kristallographie*, **229**, 345–352.

Petříček V., Eigner V., Dušek M. and Čejchan A. (2016) Discontinuous modulation functions and their application for analysis of modulated structures with the computing system JANA2006. *Zeitschrift für Kristallographie*, **231**, 301–312.

Plášil J. (2018) The super-space approach to the structures of selected U^{6+} minerals and compounds. *Aperiodic* 2018 (9th Conference on Aperiodic Crystals), Abstract 56.

Plášil J, Petříček V., Locock A.J., Škoda R. and Burns P.C. (2017) The (3 + 3) commensurately modulated structure of the uranyl silicate mineral swamboite-(Nd), $Nd_{0.333}[(UO_2)(SiO_3OH)](H_2O)_{2.41}$. *Zeitschrift für Kristallographie*, **233**, 223–232.

Pouchou J.L. and Pichoir F. (1985) "PAP" φ(ρZ) procedure for improved quantitative microanalysis. Pp. 104–106 in: *Microbeam Analysis* (J.T. Armstrong, editor). San Francisco Press, California.

Rigaku (2018) *CrysAlis CCD and CrysAlis RED*. Rigaku-Oxford Diffraction Ltd, Yarnton, Oxfordshire, UK.

Sidorenko G.A., Chistyakova N.T., Chukanov N.V., Naumova I.S. and Rossulov V.A. (2005) Carcurmolite: New data on chemical composition and constitution the mineral. *New Data on Minerals*, **40**, 29–36.

Stevens B.P.I, Barnes R.G. and Forbes B.G., (1990) Willyama Block – regional geology and minor mineralisation. Pp. 1065–1072 in: *Geology of the Mineral Deposits of Australia and Papua New Guinea* (F.E. Hughes, editor). Australasian Institute of Mining and Metallurgy, Monograph Series, **14**.

Zhang J. and Guo Y. (2012) Preparation and characterization of large-sized ADM monocrystals. *Applied Mechanics and Materials*, **152–154**, 126–129.